Article

Fiber-Dependent and -Independent Toxicity of Islet Amyloid Polypeptide

Diana E. Schlamadinger[1] and Andrew D. Miranker[1,*]
[1]Department of Molecular Biophysics and Biochemistry, Yale University, New Haven, Connecticut

ABSTRACT The 37-residue peptide hormone islet amyloid polypeptide (IAPP) plays a central role in diabetes pathology. Although its amyloid fiber aggregation kinetics and cytotoxicity to β-cells are well documented, few reports have directly assessed the role of fibers in cell-based toxicity experiments. Here, we report that amyloid formation of IAPP can be strongly inhibited by the extracellular environment of live cells. For example, fiber formation is more strongly suppressed in cell culture medium than in aqueous buffer. The serum component of the medium is responsible for this inhibition. Although amyloid formation was previously shown to be catalyzed by both synthetic and chloroform-extracted phospholipid surfaces, it is instead inhibited by membrane surfaces prepared directly from the plasma membranes of an immortal β-cell line. This disparity is reconciled by direct assessment of fibers in cell-culture-based toxicity experiments. We discovered that fibers are nontoxic if they are washed free of adsorbed nonfibrillar components. Moreover, toxicity is not only rescued when monomers are added back to fibers but is greater than what is observed from the precursor alone. Our results are interpreted in light of the capacity of the fiber surface to template amyloid nucleation.

INTRODUCTION

A critical characteristic of type II diabetes is the dysfunction and subsequent death of insulin-secreting β-cells of the pancreas. The 37-residue peptide hormone islet amyloid polypeptide (IAPP) is thought to play a central role in diabetes pathology because more than 90% of diabetes patients possess IAPP amyloid deposits (1,2), and rodents transgenic for human IAPP (hIAPP) exhibit spontaneous β-cell dysfunction and development of diabetes-like symptoms, including elements of early progression such as insulinitis (3). Challenges in the treatment of type I diabetes through islet cell transplantation have also been attributed to the amyloidogenic properties of this hormone (4).

IAPP possesses a broad range of conformations and activities that are strongly dependent on its environment. IAPP is a natively unstructured peptide that readily forms amyloid fibers rich in β-sheet. IAPP also readily binds anionic phospholipid bilayers, with model lipid membranes typically reported as strong accelerants of fiber assembly. This may be relevant to disease, as a rise in anionic lipid (e.g., phosphatidic acid) content has been associated with metabolic changes in diabetes (5,6). Other relevant factors may include insulin (7), vesicle curvature (8), pH (9,10), ionic strength (11), and nonanionic lipids (8). Upon binding, IAPP adopts a predominantly α-helical structure that spans the first ~22 residues of the sequence (12–14). Helicity is observed in stabilized IAPP structures that permit leakage of synthetic vesicles via pore formation (15,16). Fiber-induced membrane disruption by IAPP has also been reported (17).

IAPP is toxic to β-cells (18,19), crosses the cellular bilayer, and localizes to mitochondria (18,20). Independent studies have reported that intermediate, oligomeric structures are responsible for toxicity (19,21). In a previous study, we established an indirect connection between membrane-bound structures and toxicity to β-cells by observing toxicity from IAPP mutants that form membrane-associated helical structure, but do not form amyloid (18). It is important to note that we and others (18,22) have shown that mutants that disable the propensity for β-sheet formation also have a diminished capacity for toxicity. A reduction of IAPP-induced toxicity has also been observed in the presence of small molecules that target and bind helical structures (23).

The most common approach for correlating membrane activity to toxicity of IAPP is to use synthetic lipid vesicles. This creates a conflict because biophysical investigation drives the selection of lipid components that enhance timescales or signal/noise ratios to facilitate mechanistic interpretation. Sensitivity to cellular conditions is typically addressed by measuring trends as a function of changes in lipid content, such as surface charge or inclusion of cholesterol. In our own work, we have shown that IAPP binding to synthetic membranes ceases below 50% anionic lipid content (24). Others have similarly reported a loss of membrane-inducible structure at an anionic lipid content of less than 50% (22). Cell membranes contain much less than 50% anionic content, and yet in previous studies we quantitatively reported surface adsorption by IAPP in cell culture on the 120 min timescale (18). Those studies were conducted with live cells under conditions in which cellular uptake mechanisms were suppressed. We reported that under toxic

Submitted May 8, 2014, and accepted for publication September 22, 2014.
*Correspondence: andrew.miranker@yale.edu
Editor: Huey Huang.

0006-3495/14/12/2559/8 $2.00
http://dx.doi.org/10.1016/j.bpj.2014.09.047

cellular conditions, such adsorption is followed by cell-penetrating peptide (CPP)-like translocation of the plasma and/or lysosomal membrane, localization to the mitochondrial compartment, followed by mitochondrial dysfunction and subsequent cell death (18).

Engel et al. (17) reported observables wholly at odds with such a model. Specifically, they concluded that fibril growth at the surface of a vesicle leads directly to membrane disruption, and suggested this as a physical basis for downstream toxicity. These disparate findings highlight the need to not only find a more representative model lipid membrane but to also directly investigate the relationship between membrane activity, fibers, and toxicity of IAPP.

MATERIALS AND METHODS

Materials

Chemicals were purchased from Sigma Aldrich (St. Louis, MO) unless otherwise specified. Synthetic IAPP was purchased from Genscript (Piscataway, NJ) and the W.M. Keck facility (New Haven, CT). The protein included the naturally occurring C-terminal amidation and an oxidized disulfide bond between residues 2 and 7 at >98% purity. Protein stocks were generated as described previously (18) but for the use of 50% acetonitrile/0.2% formic acid as eluent from a MacroSpin column (The Nest Group, Southborough, MA). This stock was split into aliquots, lyophilized, and stored at −80°C. Aliquots were dissolved with water to 1 mM or 200 μM and used immediately in cell-based or kinetics experiments. The lipids 1,2-dioleoyl-*sn*-glycero-3-phosphocholine (DOPC) and 1,2-dioleoyl-*sn*-glycero-3-phospho-(1′-*rac*-glycerol) (DOPG, sodium salt) were purchased from Avanti Polar Lipids (Alabaster, AL), and vesicles were extruded with 100 nm filters (23). Alexa-488 carboxylic acid, succinimidyl ester was purchased from Life Technologies (Carlsbad, CA).

IAPP fibers ($IAPP_{fib}$) were generated by incubating 50 μM hIAPP in 50 mM sodium phosphate buffer, 100 mM KCl, pH 7.4, for ~15 h. Fibers were pelleted at 21,000 *g* for 30 min and resuspended three times using water. After the final spin, the pellet was resuspended to create a 1 mM (monomeric units and assuming no loss) stock of fibers. This stock, as well as a diluted 100 μM stock in water, was made fresh on the same day for each cell-viability or kinetic assay.

Alexa-488-labeled IAPP was prepared as described previously (18). Briefly, IAPP was incubated with Alexa-488 carboxylic acid, succinimidyl ester on a MacroSpin column for 4 h. Labeled IAPP was eluted from the MacroSpin column with 50% acetonitrile/0.2% formic acid solution. This was then diluted with 7 M guanidinium hydrochloride solution to a total organic content of <5%. Labeled protein was then purified by reverse-phase high-performance liquid chromatography, and identity was confirmed by Fourier transform ion cyclotron resonance (FT-ICR) mass spectrometry. Aliquots were lyophilized and stored at −80°C. Stocks at 120 μM in water were prepared and used immediately before imaging experiments.

Kinetic assays

For experiments measuring the effects of cell culture media, reactions were initiated by dilution of protein stock solution into 50 mM sodium phosphate buffer (100 mM KCl, pH 7.4) containing 100–200 nM thioflavin T (ThT; Acros Organics, Geel, Belgium). For experiments measuring the effects of giant plasma membrane vesicles (GPMVs), reactions were initiated in 10 mM HEPES buffer (150 mM NaCl, 2 mM $CaCl_2$, pH 7.4) containing 250 nM ThT. Formation of amyloid was monitored by fluorescence (excitation 450 nm, emission 485 nm) in nonbinding black 96-well plates (Greiner BioOne, Monrose, NC) using a FluoDia T70 fluorescence plate reader (Photon Technology International, Birmingham, NJ). Each kinetic trace was fit to a sigmoidal form:

$$I = \frac{(b_2 + m_2 t) + (b_1 + m_1 t) e^{\frac{t50 - t}{\tau}}}{1 + e^{\frac{t50 - t}{\tau}}}$$

where I is the fluorescence intensity, t is time, and b, m, and τ are dependent fitting variables. The parameter t_{50} represents the time at which fiber formation is midway between the upper and lower baselines extended, and corresponds to an inflection point if the upper and lower baselines are parallel. All samples were run in triplicate and error bars represent standard deviations.

Cell culture

Rat insulinoma INS-1 cells (832/13; Dr. Gary W. Cline, Department of Internal Medicine, Yale University) were cultured at 37°C and 5% CO_2 in phenol-red-free RPMI 1640 medium supplemented with 10% fetal bovine serum, 1% penicillin/streptomycin (Life Technologies), and 2% INS-1 stock solution (500 mM HEPES, 100 mM L-glutamine, 100 mM sodium pyruvate, and 2.5 mM β-mercaptoethanol). Cells were passaged when they reached ~95% confluence (0.25% Trypsin-EDTA; Life Technologies).

COS-1 cells (from immortalized African green monkey kidney; CRL-1650 ATCC) were cultured at 37°C and 5% CO_2 in Dulbecco's modified Eagle's medium supplemented with 10% fetal bovine serum and 1% penicillin/streptomycin (all from Life Technologies). Cells were passaged when they reached ~95% confluence (0.25% Trypsin-EDTA; Life Technologies).

GPMV isolation

GPMVs were isolated from INS-1 and COS-1 cells according to established methods (25). Briefly, cells were plated in 35 mm dishes and cultured for 48 h. Cells were washed with a 10 mM HEPES, 150 mM NaCl, 2 mM $CaCl_2$ (pH = 7.4) twice and were then exposed to 10 mM N-ethyl maleimide (NEM; Sigma Aldrich) for 1 h (COS-1 cells) or 2 h (INS-1 cells). Cells exposed to 10 mM HEPES, 150 mM NaCl, 2 mM $CaCl_2$ (pH = 7.4) for the same time period (NEM− samples) served as a background control. Both NEM− and NEM+ samples were removed via pipet from dishes after the incubation period and further concentrated to matched volumes using spin concentrators (3 kDa and 100 kDa molecular mass cutoff; Millipore, Billerica, MA). Aliquots of NEM− and NEM+ samples were taken after zero, one, and two 5- to 10-min spins at 2880 *g* (3 kDa cutoff) or 720 *g* (100 kDa cutoff) and used in kinetic reactions. Total phosphate was measured in the most concentrated NEM− and NEM+ samples and in synthetic lipid vesicle stocks as previously described (16). The phosphate content in NEM− samples was below the detection limit of the assay.

GPMV imaging

Images were acquired in wide-field mode on an in-house-built inverted microscope as described previously (26). Fluorescent imaging was achieved with wide-field illumination at 488 nm. The camera gain and exposure time settings were matched between images. Samples for imaging were prepared by mixing 60 μL of NEM+ or NEM− material and 2.5 μM Alexa-488 IAPP (in pure water) into 10 mM HEPES, 150 mM NaCl, 2 mM $CaCl_2$ (pH = 7.4) buffer (total volume = 300 μL). Samples were incubated 30 min before imaging.

Cell viability

Cell viability was measured colorimetrically using the Cell-Titer Blue (CTB; Promega, Madison, WI) fluorescence-based assay. Cells were plated at a density of 5000 cells/well in 96-well plates (BD Biosciences, San

Diego, CA). Peptide was directly introduced to each well 24 h after passaging and plating, and then further incubated for an additional 72 h. After the incubation period, 20 μL CTB reagent was added to each well and incubated at 37°C and 5% CO_2 for 2.5–3.5 h. The fluorescence of the resorufin product was measured on a FluoDia T70 fluorescence plate reader (Photon Technology International, Birmingham, NJ). All wells included the same amount of water to account for different concentrations of peptide added to sample wells. Wells that included water vehicle, but not peptide, served as the negative control (0% toxic), and wells containing 10% DMSO served as the positive control (100% toxic). Percent toxicity was calculated using the following equation:

$$\%Toxicity = 100 - \left[100 \cdot \left(\frac{\langle S\rangle - \langle P\rangle}{\langle N\rangle - \langle P\rangle}\right)\right]$$

Each independent variable is the average fluorescence of eight plate replicates from the negative control ($\langle N\rangle$), positive control ($\langle P\rangle$), and samples ($\langle S\rangle$). Results presented for viability experiments are an average of three independent experiments (i.e., 24 replicates total). Error bars represent the standard error of the mean of the three independently conducted experiments.

RESULTS

Little is known about how environments that are obligatory for measurement influence the membrane activity and amyloidogenic nature of IAPP. Here, we designed experiments to address how the extracellular environment of live cells influences de novo and seeded amyloid assembly. We utilized a model membrane vesicle system derived directly from a pancreatic β-cell line and assessed the influence of the membrane on amyloid kinetics. The toxicity of soluble IAPP, preformed fibers, and soluble IAPP in the presence of preformed fibers was compared quantitatively.

Environments that are important for cell-based experiments strongly inhibit IAPP fiber formation. We initiated fiber kinetics by diluting a 1 mM protein stock solution in water into buffer. At a final protein concentration of 40 μM in 50 mM phosphate buffer and 100 mM KCl (pH = 7.4), the midpoint, t_{50}, of such an assembly reaction is 10,300 ± 500 s. In marked contrast, the same reaction performed in 96% RPMI medium resulted in no detection of amyloid assembly. Inhibition by RPMI medium is dose dependent, with as little as 0.4% medium (99.6% phosphate buffer) yielding inhibition of t_{50} > 2-fold (Fig. 1). At 2% RPMI medium, the t_{50} is beyond our timescale of monitoring (>14 hr). Omission of the fetal bovine serum component of RPMI medium results in a rate of IAPP conversion to fiber similar to that observed in buffer alone (Fig. 1 *b*), indicating that the protein fraction is responsible for inhibition. Purified albumin (bovine and human, 0.6 μM) extended relative t_{50} values to 2.6 ± 0.1 and 2.5 ± 0.1, respectively, compared with a reaction conducted in the absence of albumin. The concentration of bovine serum albumin (BSA) present in 1% RPMI is 0.6 μM (Fig. S1 in the Supporting Material), suggesting that other components of the serum fraction are relevant to the inhibitory properties of the medium. Since β-cells surround capillaries and

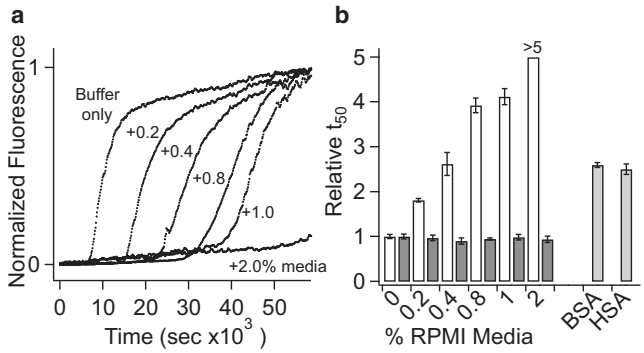

FIGURE 1 Cell culture medium inhibits hIAPP fiber formation. Fiber formation is initiated by dilution of hIAPP stock in water to 40 μM in reactions containing 50 mM phosphate buffer and 100 mM KCl (pH = 7.4) diluted to the indicated percentage of medium (RPMI, phenol-red free). (*a*) Representative normalized kinetic traces (monitored using 100 nM ThT fluorescence) are presented. (*b*) Statistics of reaction midpoints, t_{50}, from repeat analyses of *a*. Open bars are t_{50} values (45 μM hIAPP) obtained for reactions at the indicated percentage of culture medium divided by the t_{50} of buffer-only reactions. Dark gray bars are the relative t_{50} obtained for reactions containing RPMI medium without the fetal bovine serum component. Light gray bars are the relative t_{50} values of a reaction in buffer containing 0.6 μM purified bovine or human serum albumin. This corresponds to a concentration approximately equivalent to that present in 2% RPMI cell culture medium.

secrete into the circulatory system, IAPP is released into an environment in which an amyloid inhibitor (albumin) is already present at high concentrations (27).

Plasma-membrane-derived vesicles isolated from cultured mammalian cells inhibit fiber formation. We prepared GPMVs from INS-1 cells according to established methods, using NEM as the vesiculating reagent (25). NEM was chosen as the reagent to generate GPMVs because it is a comparatively mild, irreversible blocker of free sulfhydryls that are present predominantly, if not exclusively, on proteins. Alternative protocols use a relatively strong, nonspecific cross-linking mixture, 25 mM paraformaldehyde/2 mM dithiothreitol (PFA/DTT). Moreover, working with both the blocker and cross-linking systems revealed that trace components of the PFA/DTT mixture could affect IAPP reaction t_{50} values (not shown). However, NEM has no effect on the t_{50} of IAPP (Fig. S2). Our reference reaction (NEM cell free) is a 40 μM IAPP fiber formation reaction in 10 mM HEPES, 150 mM NaCl, 2 mM $CaCl_2$ (pH = 7.4), and 10 mM NEM (Fig. 2) and has a t_{50} of 18,900 ± 400 s. In the absence of vesiculant, the reaction has a t_{50} of 18,100 ± 200 s, indicating that the vesiculant has no independent effect on the conversion rate. The HEPES buffer is the standard buffer system used for GPMV isolation, and therefore the absolute t_{50} values reported for GPMV experiments differ slightly from those reported in the phosphate buffer system (see above). Given the inhibitory nature of the cell culture medium described above, cells were washed extensively before incubation with vesiculant. Moreover, the t_{50} was compared with

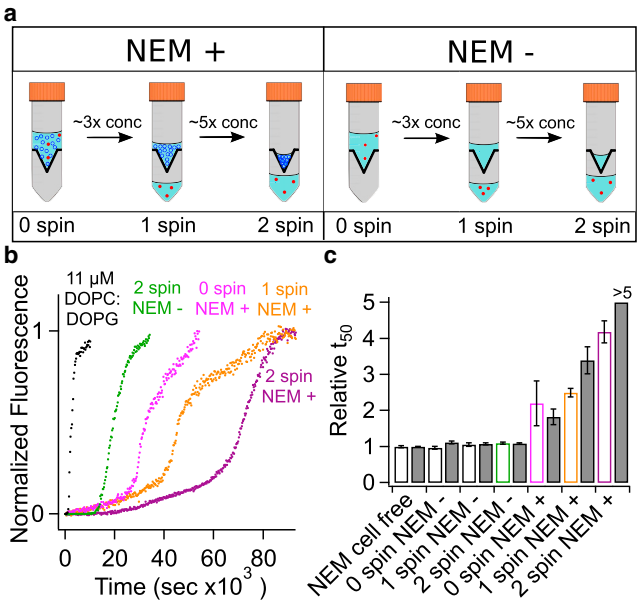

FIGURE 2 Cell-derived plasma membrane vesicles inhibit fiber formation. GPMVs were used as a reagent added to standardized 40 μM IAPP fiber formation reactions. (*a*) Schematic depicting the stepwise concentration of GPMVs using a 100 kDa molecular mass cutoff centrifugal concentrator for both NEM+ and NEM− samples. GPMVs are depicted as blue open circles, and residual medium components are depicted as red dots. (*b*) Representative kinetic traces are shown for the GPMVs added directly to the fiber formation reaction (zero spin, NEM+), and for washes that have been concentrated ~3× (one spin, NEM+) and ~15× (two spins, NEM+). For comparison, vesicle-free conditions were created using washes that did not contain the vesiculating reagent (two spins, NEM−). A representative trace is shown in which 11 μM 50:50 DOPC/DOPG synthetic lipid vesicles (in monomer units) were prepared in the same buffer. (*c*) Statistics of reaction midpoints, t_{50}, from fits to repeated analyses of *b*. Open bars are data from INS-1 GPMVs. Solid bars indicate data from analyses using COS-1 GPMVs. A further control is shown from NEM-containing samples that were never in contact with cells (NEM cell free). In panels *b* and *c*, green corresponds to the two-spin NEM− sample, pink corresponds to the zero-spin NEM+ sample, orange corresponds to the one-spin NEM+ sample, and purple corresponds to the two-spin NEM+ sample. To see this figure in color, go online.

solutions derived by procedures that were identical in every respect except for the omission of NEM (indicated as NEM− samples). Inhibition by materials gathered by this procedure can be attributed to the GPMVs using a dose-response assay. We concentrated the GPMV isolate (NEM+ samples) stepwise using a 100 kDa molecular mass cutoff centrifugal concentrator to pass many soluble proteins originating from the medium while concentrating the GPMVs (Fig. 2 *a*). A representative example (Fig. 2 *b*) clearly shows that concentration of the GPMVs yields a dose dependence. We also observed a similar dose-dependent extension of t_{50} using a 3 kDa molecular mass cutoff centrifugal concentrator (Fig. S3). Repeats at 100 kDa show relative t_{50} values delayed by factors of 2.2 ± 0.6, 2.5 ± 0.1, and 4.2 ± 0.3, respectively (Fig. 2 *c*). Since NEM− samples do not modulate the t_{50} of IAPP reactions compared with our reference reaction, residual media components from the GPMV isolation procedure are unlikely contributors to the inhibition observed by NEM+ samples (GPMV-containing samples).

Inhibition by GPMVs is not cell-line specific. Insulin and rodent IAPP, both of which are secreted by INS-1 cells, inhibit IAPP fiber formation (7,28). To determine whether GPMV inhibition is cell-line specific, we repeated the assays using GPMVs isolated from COS-1 cells, a kidney cell line derived from African green monkey (Fig. 2 *b*). Relative t_{50} values extended to 1.8 ± 0.2, 3.4 ± 0.4, and >5 in NEM+ samples, further indicating that the GPMV-induced t_{50} extension is not a result of inhibition by residual rodent IAPP or insulin secreted by INS-1 cells. Higher relative t_{50} values in the presence of COS-1 GPMVs compared with INS-1 GPMVs is likely a result of a slightly higher concentration of GPMVs isolated from COS-1 cells (see below). The progression of average relative t_{50} values in the presence of INS-1 NEM− samples remained largely unchanged, with values of 1.0 ± 0.1, 1.1 ± 0.1, and 1.1 ± 0.1. The average relative t_{50} values obtained for COS-1 NEM− samples were 1.1 ± 0.1, 1.1 ± 0.1, and 1.1 ± 0.1. GPMV isolates plainly extended the t_{50} of IAPP regardless of cell type.

GPMV inhibition of fiber formation kinetics is in direct contrast to the catalysis observed by synthetic lipid vesicles. Kinetics in the presence of 50:50 DOPC/DOPG lipid vesicles at similar total phosphate concentrations show a strong enhancement of fiber kinetics of 40 μM IAPP (Fig. 2 *a*). Reactions containing DOPC/DOPG lipid vesicles with 11 μM total phosphate reduce the t_{50} 5-fold compared with the t_{50} measured in a reference sample. In this work, total phosphate serves as an indirect measure of lipid concentration in GPMVs. The phosphate content for each INS-1 GPMV NEM+ sample was 2, 7, and 35 μM, respectively. The phosphate content for each COS-1 GPMV NEM+ sample was 4, 12, and 60 μM, respectively. Plainly, we observe a reduction of the t_{50} of IAPP in the presence of synthetic liposomes, and an extension of t_{50} in the presence of cell-derived liposomes at total phospholipid concentrations that are semi-quantitatively matched.

To further support the role of GPMVs in these assays, we directly determined that IAPP binds both INS-1 and COS-1 GPMVs (Fig. 3). We imaged GPMVs with laser and white-light illumination using wide-field fluorescence microscopy. Alexa-488-labeled IAPP was observed to localize uniformly to the surface of INS-1 GPMVs and occasional contaminating dead cells (Fig. 3, *top*). For this work, we regard dead cells as an equivalent reagent to GPMVs. Labeled IAPP also localizes to the surface of COS-1 GPMVs (Fig. 3, *bottom*). NEM− control samples showed no GPMVs and had high background from the labeled IAPP under matched detector settings (not shown), consistent with IAPP partitioning to GPMVs in NEM+ samples. The Alexa-488 images of NEM+ material depict a relatively

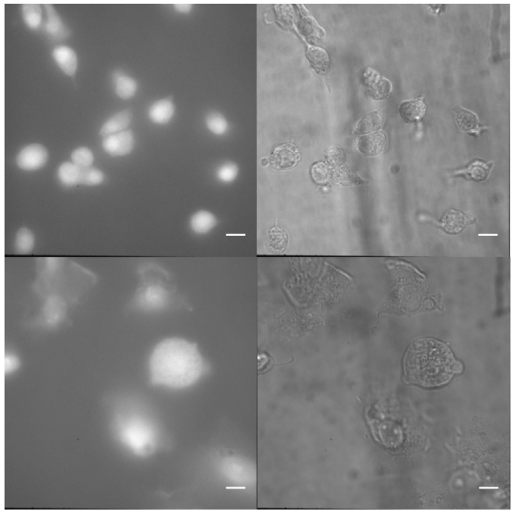

FIGURE 3 IAPP binds GPMVs. Samples were prepared as described in Fig. 2 except for the addition of 2.5 μM-labeled IAPP. Representative white-light (*right*) and fluorescence (*left*) image pairs are shown for GPMVs derived from INS-1 cells (*top*) and COS-1 cells (*bottom*), respectively. Scale bar is 10 μm.

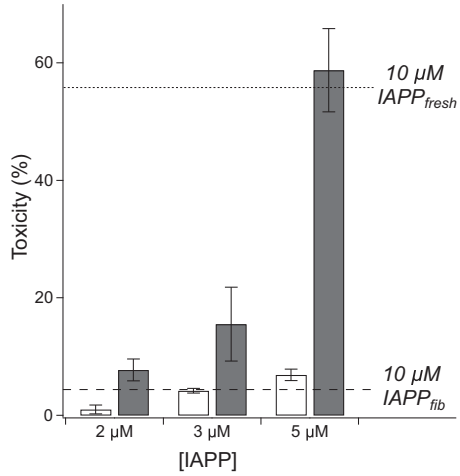

FIGURE 4 The toxicity of fresh IAPP is increased by addition of nontoxic fibers. IAPP toxicity to INS-1 cells was measured colorimetrically 72 h after exposure to the indicated total (fiber + monomer) concentration of IAPP. Cells were exposed to $IAPP_{fresh}$ (*open bars*) or 1 μM of preformed $IAPP_{fib}$ mixed with $IAPP_{fresh}$ (*gray bars*). Horizontal lines are drawn at the toxicity levels measured for 10 μM $IAPP_{fresh}$ (56% $\pm$ 6%, *dotted*) or 10 μM $IAPP_{fib}$ (5% $\pm$ 2%, *dashed*).

uniform distribution of IAPP on the membrane surface, which is consistent with observations on the surface of GUVs made from chloroform/methanol-extracted lipids (29). We previously reported that IAPP forms fluorescent puncta on live cells (18). This suggests that puncta formation that is large enough to be resolved by wide-field microscopy may be a live-cell-specific result. Overall, our observations clearly indicate that IAPP binds our plasma-membrane-derived GPMVs.

Freshly prepared IAPP dissolved in pure water ($IAPP_{fresh}$) is toxic to INS-1 cells. As a function of peptide concentration, toxicity is sigmoidal (Fig. S4 *a*). $IAPP_{fresh}$ reduced cell viability by 1.0% $\pm$ 0.7% (2 μM), 4.2% $\pm$ 0.4% (3 μM), 7% $\pm$ 1% (5 μM), and 56% $\pm$ 6% (10 μM) after 72 h incubation (Fig. 4), which are comparable to previously published toxicities of IAPP to INS-1 cells (18). Experiments conducted with a different synthetic batch of IAPP and different style well plates showed a slightly lower toxicity (~13 μM elicited 50% toxicity; Fig. S4 *a*). Indeed, we routinely assessed the dose response of all lots of synthetic and expressed IAPP, as variation in the EC_{50} on the order of 2- to 3-fold is common between lots.

IAPP fibers ($IAPP_{fib}$) are not toxic to cells. Application of 10 μM $IAPP_{fib}$ directly to the cell culture medium showed little toxicity compared with the same concentration of freshly dissolved peptide (Fig. 4). Importantly, since our preformed amyloid fibers were grown in phosphate buffer, washed, and then concentrated in water, the resulting treated fibers reduced cell viability by only 5% $\pm$ 2%. Treated fibers used in cell-viability assays retained the capacity to affect amyloid kinetics reactions. Seeded kinetics wholly bypassed the lag phase of the de novo kinetics profile but still retained a profile with a lag phase (Fig. S5). Moreover, the slope of the profile at the t_{50} was far greater than that calculated for assembly governed only by primary nucleation. Both of these characteristics are consistent with secondary (fiber-dependent) nucleation as observed previously for IAPP (30,31).

Fiber-based toxicity can be rescued. When treated fibers were added simultaneously with freshly dissolved protein ($IAPP_{fresh}$ + $IAPP_{fib}$), cell viability was greatly reduced compared with the same amount of freshly dissolved protein alone (Fig. 4). Cell viability was reduced by 8% $\pm$ 2% (1 μM $IAPP_{fresh}$ + 1 μM $IAPP_{fib}$), 16% $\pm$ 6% (2 μM $IAPP_{fresh}$ + 1 μM $IAPP_{fib}$), and 59% $\pm$ 7% (4 μM $IAPP_{fresh}$ + 1 μM $IAPP_{fib}$). Note that the concentration of $IAPP_{fib}$ in experiments that included $IAPP_{fresh}$ + $IAPP_{fib}$ is 10 times less than the amount used to measure toxicity of $IAPP_{fib}$ directly as described above. A strong reduction in cell viability was also observed when the experiment was conducted with a different lot of IAPP and well-plate format (Fig. S4 *b*).

Toxicity in the presence of fibers is unlikely to be the result of elongation (Fig. 5). As with the de novo kinetics, the cell culture medium halted the seeded fiber kinetics of IAPP. In the presence of 2 μM $IAPP_{fib}$, as little as 4% medium (96% buffer) extended the t_{50} of a seeded reaction nearly 3-fold compared with the reaction initiated in phosphate buffer alone. This inhibition was potent, albeit not as potent as de novo inhibition, in which as little as 0.4% medium was sufficient to suppress amyloid formation by a comparable amount (Fig. 1). A critical difference is that the cell-based experiments were conducted in 100% medium, a 10-fold lower concentration of $IAPP_{fresh}$, and a 2-fold lower concentration of $IAPP_{fib}$. We previously reported that β-cell uptake of IAPP in culture medium is complete

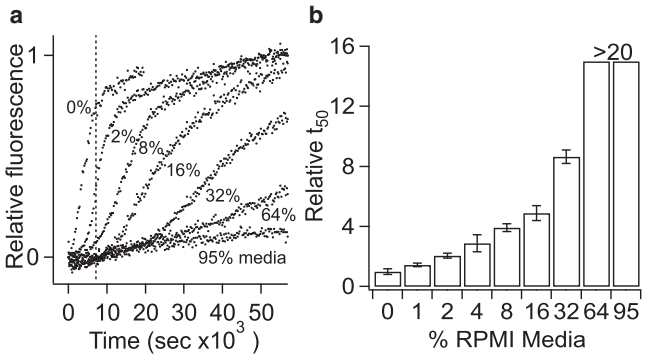

FIGURE 5 The medium inhibits fiber formation seeded with preformed fibers. (*a*) Representative normalized kinetic traces for 40 μM $IAPP_{fresh}$, 2 μM $IAPP_{fib}$, and the indicated percentage of RPMI medium. The dotted line demarcates the time taken for 10 μM $IAPP_{fresh}$ (a toxic concentration) to partition from the medium to cultured cells (18). (*b*) Statistics of reaction midpoints, t_{50}, from fits to repeat analyses of (*a*).

within 2 h (Fig. 5 *a*, *vertical dotted line*) (18). It is likely, therefore, that soluble peptide is taken up by cells long before extracellular conversion to amyloid occurs.

DISCUSSION

It is particularly challenging to associate molecular structure with gains of toxic function in amyloid systems with disordered peptide precursors. Multiple conformers and oligomeric states are populated and interconvert, resulting in several gains of function that act together to contribute to cell death. In this study, we investigated the impact of the extracellular environment on the amyloid fiber assembly of IAPP and the role of preamyloid states in assembly and toxicity. Our observations provide a very new perspective. Specifically, 1) the medium used to culture cells strongly suppresses amyloid formation; 2), giant vesicles generated from the plasma membrane of cultured cells suppress amyloid formation; 3), IAPP fibers are nontoxic provided they are washed free of precursor; and 4), combinations of fiber and monomer act synergistically to elicit greater toxicity than would either component alone. Our findings clearly point to a critical role for fibers in gains of toxic function. However, it is not the fibers per se that are toxic; rather, it is their capacity to catalyze the formation of toxic species from precursor material that is relevant.

Primary toxicity can be defined as deriving from toxic species that form independently of preexisting fibers. The cellular environment, including media and vesicles prepared from plasma membrane, strongly delays amyloid kinetics, and fibers possess no intrinsic toxicity. This suggests that, at least in cell culture, extracellular fiber formation is not a requirement for toxicity. Our results do not exclude the possibility that once IAPP is inside cells, amyloid formation occurs, resulting in toxicity. However, toxicity is also observable from a rodent sequence variant of IAPP with no evidence of fiber formation. Not only is rodent IAPP capable of toxicity, but it follows a time course and subcellular localization profile comparable to that observed for the readily amyloidogenic human protein (18).

Secondary toxicity, conceptually similar to secondary nucleation, can be defined as formation of toxic species that is dependent on the presence of preformed fibers. The notion that the presence of fibers is required for toxicity is strongly supported by studies showing that membrane-catalyzed amyloid formation by IAPP coincides with a loss of membrane integrity (17). Moreover, it has been observed that protein preincubated into the lag phase of its amyloid conversion enhances the formation of toxic species (32). The latter studies permit the inference that either nonfibrillar toxic oligomers are created in the lag period or, alternatively, primary nucleation dominates over secondary nucleation in the lag phase, generating low populations of fiber. Here, we directly assessed secondary toxicity by first showing that preparations of amyloid were nontoxic. We then rescued toxicity by mixing subtoxic quantities of soluble and fibrous IAPP into the cell culture (Fig. 5). This behavior strongly suggests that although the fibers themselves are nontoxic, they can behave as catalysts for the formation of toxic species.

The origin of apparent secondary toxicity remains unclear. One possibility is that secondary toxicity is directly related to nonbreakage forms of secondary nucleation, or the capacity of an amyloid fiber to act as a catalytic surface for the formation of new fibers from precursor material (30,31). IAPP and other systems possess kinetic profiles that require such secondary processes. In Aβ from Alzheimer's disease, Cohen et al. (30) observed secondary toxicity in human neuroblastoma cells. They found that Aβ toxicity was predominantly elicited from monomeric peptide (4 μM) in the presence of fibers (40 nM) rather than by monomeric peptide alone. As oligomers were observed during the kinetics analysis, the fiber-dependent toxicity in the presence of freshly dissolved peptide was attributed to the catalyzed generation of directly observed toxic oligomeric species. IAPP and Aβ are similar in length, physicochemical properties, and sequence (33). These similarities have been recognized and resulted in diverse observations, such as suppression of Aβ self-assembly by IAPP mimics (34) and cocrystal structures of Aβ and IAPP bound to insulin-degrading enzyme (35). Therefore, we conjecture that oligomeric species that rapidly populate in the presence of preformed Aβ fibers (30) may also be generated by mixtures of $IAPP_{fresh}$ and $IAPP_{fib}$. Unlike the case with Aβ, however, nonamyloid, toxic oligomer preparations of IAPP have yet to be purified. For both Aβ and IAPP, secondary toxicity is stronger than primary toxicity. Collectively, these findings implicate secondary toxicity as the dominant component of amyloid precursor-induced cellular dysfunction.

The inhibition of fiber formation by GPMVs was wholly unexpected. Several labs, including our own, have reported and characterized the catalysis of IAPP amyloid formation

by anionic phospholipid bilayers (8,24,36). However, the lipid and cholesterol content, net lipid charge, and size of the lipid vesicle all affect fiber kinetics differently. Larger vesicles that do not contain any anionic lipid vesicles or include cholesterol extend fiber kinetics, whereas smaller lipid vesicles that contain anionic lipids accelerate IAPP fiber kinetics (8). Studies in this area have led to models of binding, pore formation, translocation, and catalysis (16,18,37), and, importantly, identified protein structures rich in α-helix. Here, we recapitulated these observables by showing the catalytic behavior of synthetic anionic lipid vesicles at total phosphate concentrations comparable to what was assessed using GPMVs. Previous studies have shown that unilamellar vesicles generated from lipids isolated by chloroform extraction from INS-1 cells (29), whole pancreas from a diabetic human, or whole chicken liver (24) catalyzed IAPP amyloid formation. Plainly, some other factor within the plasma membrane is relevant to inhibition. This may include a component that is excluded by solvent extraction, such as protein, an as-yet-unidentified lipid component, or a physical property such as curvature. Here, we observed IAPP binding to cell-derived membrane, whereas others have seen IAPP binding to membrane from chloroform-derived GUVs (29). However, two-component, synthetic large unilamellar vesicles matched to the typical net charge of cell membranes did not show any binding (24). Therefore, we assert that both lipids and proteins affect catalysis, but conjecture that surface-expressed protein components play an underappreciated role in plasma membrane binding.

CONCLUSIONS

We observe that preformed fibers are not a toxic species, but rather elicit toxicity when combined with freshly dissolved IAPP. This secondary toxicity is quantitatively stronger than the toxicity observed with freshly dissolved IAPP (primary toxicity) alone, and may be an important feature of diabetic pathology. We conjecture that this toxicity is derived from the amyloid fiber surface-based catalysis that is evident in IAPP and Aβ systems. We base our conclusions on a surprising observation, namely, that both the extracellular environment and plasma membrane of cells strongly suppress amyloid conversion. This finding is in direct contrast to many observations that membranes composed of synthetic lipid catalyze the formation of fibers. We propose that the lipid vesicles described in this work can be used to study binding, disorder-to-order structural transitions, membrane disruption, translocation, and pore-formation gains of function by IAPP.

SUPPORTING MATERIAL

Five figures and Supporting References are available at http://www.biophysj.org/biophysj/supplemental/S0006-3495(14)01114-X.

We thank Prof. Gary Cline for the initial gift of the INS-1 cells, Prof. Elizabeth Rhoades and Dr. Sylvain Zorman for discussions and assistance with imaging, Dr. Yulia Surovtseva and Dr. Jane Merkel for helpful discussions and assistance with cell culture, and Prof. Mark Johnson and Dr. Christopher Johnson for assistance and use of the FT-ICR mass spectrometer. We are also grateful to Dr. Abhinav Nath for a careful reading of this manuscript.

This research was supported by NIH GM094693 and an American Diabetes Association mentor-based postdoctoral fellowship.

REFERENCES

1. Höppener, J. W. M., B. Ahrén, and C. J. M. Lips. 2000. Islet amyloid and type 2 diabetes mellitus. *N. Engl. J. Med.* 343:411–419.
2. Kahn, S. E., S. Andrikopoulos, and C. B. Verchere. 1999. Islet amyloid: a long-recognized but underappreciated pathological feature of type 2 diabetes. *Diabetes.* 48:241–253.
3. Matveyenko, A. V., and P. C. Butler. 2006. β-cell deficit due to increased apoptosis in the human islet amyloid polypeptide transgenic (HIP) rat recapitulates the metabolic defects present in type 2 diabetes. *Diabetes.* 55:2106–2114.
4. Potter, K. J., A. Abedini, …, C. B. Verchere. 2010. Islet amyloid deposition limits the viability of human islet grafts but not porcine islet grafts. *Proc. Natl. Acad. Sci. USA.* 107:4305–4310.
5. Farese, R. V., P. E. DiMarco, …, A. D. Morrison. 1986. Rapid glucose-dependent increases in phosphatidic acid and phosphoinositides in rat pancreatic islets. *Endocrinology.* 118:1498–1503.
6. Rustenbeck, I., A. Matthies, and S. Lenzen. 1994. Lipid composition of glucose-stimulated pancreatic islets and insulin-secreting tumor cells. *Lipids.* 29:685–692.
7. Knight, J. D., J. A. Williamson, and A. D. Miranker. 2008. Interaction of membrane-bound islet amyloid polypeptide with soluble and crystalline insulin. *Protein Sci.* 17:1850–1856.
8. Caillon, L., O. Lequin, and L. Khemtémourian. 2013. Evaluation of membrane models and their composition for islet amyloid polypeptide-membrane aggregation. *Biochim. Biophys. Acta.* 1828:2091–2098.
9. Jha, S., J. M. Snell, …, A. T. Alexandrescu. 2014. pH dependence of amylin fibrillization. *Biochemistry.* 53:300–310.
10. Abedini, A., and D. P. Raleigh. 2005. The role of His-18 in amyloid formation by human islet amyloid polypeptide. *Biochemistry.* 44:16284–16291.
11. Marek, P. J., V. Patsalo, …, D. P. Raleigh. 2012. Ionic strength effects on amyloid formation by amylin are a complicated interplay among Debye screening, ion selectivity, and Hofmeister effects. *Biochemistry.* 51:8478–8490.
12. Williamson, J. A., J. P. Loria, and A. D. Miranker. 2009. Helix stabilization precedes aqueous and bilayer-catalyzed fiber formation in islet amyloid polypeptide. *J. Mol. Biol.* 393:383–396.
13. Apostolidou, M., S. A. Jayasinghe, and R. Langen. 2008. Structure of α-helical membrane-bound human islet amyloid polypeptide and its implications for membrane-mediated misfolding. *J. Biol. Chem.* 283:17205–17210.
14. Nanga, R. P. R., J. R. Brender, …, A. Ramamoorthy. 2008. Structures of rat and human islet amyloid polypeptide IAPP(1-19) in micelles by NMR spectroscopy. *Biochemistry.* 47:12689–12697.
15. Knight, J. D., J. A. Hebda, and A. D. Miranker. 2006. Conserved and cooperative assembly of membrane-bound α-helical states of islet amyloid polypeptide. *Biochemistry.* 45:9496–9508.
16. Last, N. B., E. Rhoades, and A. D. Miranker. 2011. Islet amyloid polypeptide demonstrates a persistent capacity to disrupt membrane integrity. *Proc. Natl. Acad. Sci. USA.* 108:9460–9465.
17. Engel, M. F. M., L. Khemtémourian, …, J. W. Höppener. 2008. Membrane damage by human islet amyloid polypeptide through fibril growth at the membrane. *Proc. Natl. Acad. Sci. USA.* 105:6033–6038.

18. Magzoub, M., and A. D. Miranker. 2012. Concentration-dependent transitions govern the subcellular localization of islet amyloid polypeptide. *FASEB J.* 26:1228–1238.

19. Janson, J., R. H. Ashley, …, P. C. Butler. 1999. The mechanism of islet amyloid polypeptide toxicity is membrane disruption by intermediate-sized toxic amyloid particles. *Diabetes.* 48:491–498.

20. Lin, C. Y., T. Gurlo, …, P. C. Butler. 2007. Toxic human islet amyloid polypeptide (h-IAPP) oligomers are intracellular, and vaccination to induce anti-toxic oligomer antibodies does not prevent h-IAPP-induced β-cell apoptosis in h-IAPP transgenic mice. *Diabetes.* 56:1324–1332.

21. Bram, Y., A. Frydman-Marom, …, E. Gazit. 2014. Apoptosis induced by islet amyloid polypeptide soluble oligomers is neutralized by diabetes-associated specific antibodies. *Sci. Rep.* 4:4267.

22. Cao, P., A. Abedini, …, D. P. Raleigh. 2013. Islet amyloid polypeptide toxicity and membrane interactions. *Proc. Natl. Acad. Sci. USA.* 110:19279–19284.

23. Hebda, J. A., I. Saraogi, …, A. D. Miranker. 2009. A peptidomimetic approach to targeting pre-amyloidogenic states in type II diabetes. *Chem. Biol.* 16:943–950.

24. Knight, J. D., and A. D. Miranker. 2004. Phospholipid catalysis of diabetic amyloid assembly. *J. Mol. Biol.* 341:1175–1187.

25. Sezgin, E., H.-J. Kaiser, …, I. Levental. 2012. Elucidating membrane structure and protein behavior using giant plasma membrane vesicles. *Nat. Protoc.* 7:1042–1051.

26. Elbaum-Garfinkle, S., T. Ramlall, and E. Rhoades. 2010. The role of the lipid bilayer in tau aggregation. *Biophys. J.* 98:2722–2730.

27. Choi, S., E. Y. Choi, …, S. W. Oh. 2004. A rapid, simple measurement of human albumin in whole blood using a fluorescence immunoassay (I). *Clin. Chim. Acta.* 339:147–156.

28. Cao, P., F. Meng, …, D. P. Raleigh. 2010. The ability of rodent islet amyloid polypeptide to inhibit amyloid formation by human islet amyloid polypeptide has important implications for the mechanism of amyloid formation and the design of inhibitors. *Biochemistry.* 49:872–881.

29. Seeliger, J., K. Weise, …, R. Winter. 2012. The effect of Aβ on IAPP aggregation in the presence of an isolated β-cell membrane. *J. Mol. Biol.* 421:348–363.

30. Cohen, S. I., S. Linse, …, T. P. Knowles. 2013. Proliferation of amyloid-β42 aggregates occurs through a secondary nucleation mechanism. *Proc. Natl. Acad. Sci. USA.* 110:9758–9763.

31. Ruschak, A. M., and A. D. Miranker. 2007. Fiber-dependent amyloid formation as catalysis of an existing reaction pathway. *Proc. Natl. Acad. Sci. USA.* 104:12341–12346.

32. Weise, K., D. Radovan, …, R. Winter. 2010. Interaction of hIAPP with model raft membranes and pancreatic β-cells: cytotoxicity of hIAPP oligomers. *ChemBioChem.* 11:1280–1290.

33. O'Nuallain, B., A. D. Williams, …, R. Wetzel. 2004. Seeding specificity in amyloid growth induced by heterologous fibrils. *J. Biol. Chem.* 279:17490–17499.

34. Yan, L.-M., A. Velkova, …, A. Kapurniotu. 2007. IAPP mimic blocks Aβ cytotoxic self-assembly: cross-suppression of amyloid toxicity of Aβ and IAPP suggests a molecular link between Alzheimer's disease and type II diabetes. *Angew. Chem. Int. Ed. Engl.* 46:1246–1252.

35. Shen, Y., A. Joachimiak, …, W.-J. Tang. 2006. Structures of human insulin-degrading enzyme reveal a new substrate recognition mechanism. *Nature.* 443:870–874.

36. Jayasinghe, S. A., and R. Langen. 2005. Lipid membranes modulate the structure of islet amyloid polypeptide. *Biochemistry.* 44:12113–12119.

37. Nath, A., A. D. Miranker, and E. Rhoades. 2011. A membrane-bound antiparallel dimer of rat islet amyloid polypeptide. *Angew. Chem. Int. Ed. Engl.* 50:10859–10862.